International Journal of Nanomedicine

Dovepress
Taylor & Francis Group

Open Access Full Text Article

ORIGINAL RESEARCH

Enhanced Skin Delivery of Mussel Adhesive Protein Modified Pluronic F127 Micelles Loaded with Curcumin for Effective Topical Treatment of Psoriasis

Jiangxiu Niu[1,*], Ming Yuan[1,*], Liye Wang[1], Pei Zhang[2], Xingang Cui[3], Jucai Wang[1], Xianming Liu[1]

[1]College of Food and Drug, Luoyang Normal University, Luoyang, Henan, 471934, People's Republic of China; [2]College of Life Science, Luoyang Normal University, Luoyang, Henan, 471934, People's Republic of China; [3]Department of Research and Teaching, Luoyang Maternal and Child Health Hospital, Luoyang, Henan, 471000, People's Republic of China

*These authors contributed equally to this work

Correspondence: Pei Zhang; Xingang Cui, Email zhangpei8877@126.com; cuixingang5207@163.com

Background: Psoriasis is a long-term inflammatory skin disorder that significantly impacts the physical and psychological well-being of those affected. Curcumin (Cur) is a natural compound that holds promise for the topical management of psoriasis. However, the barrier property of the stratum corneum (SC) and the insufficient retention ability of the drug in the skin have severely restricted the clinical efficacy of Cur. To overcome these limitations, we introduced mussel adhesive protein (MAP) for its superior bioadhesive properties, and developed Cur-loaded MAP modified Pluronic F127 micelles (MAP-F127/Cur) to improve the skin permeation and retention of Cur and enhance the therapeutic effect on psoriasis.

Methods: In this study, MAP-F127 was synthesized via chemical synthesis. MAP-F127/Cur was prepared using the thin-film hydration method, and the physicochemical properties of the formulation were characterized. In addition, porcine skin was employed as an in vitro model to evaluate the skin permeation of the formulation and to elucidate the interaction mechanism between the formulation and the skin. Furthermore, the therapeutic efficacy of the formulation against psoriasis was assessed using an imiquimod-induced psoriasis mouse model.

Results: The prepared MAP-F127/Cur had a regular spherical shape and good dispersion, and could efficiently load Cur in the amorphous form. The skin retention of MAP-F127/Cur was notably elevated in comparison to both the Cur-loaded Pluronic F127 micelles (F127/Cur) and Cur solution ($p<0.01$). Studies on the skin permeation mechanism showed that MAP-F127/Cur could break through the restriction of the skin barrier by regulating lipid arrangement and keratin conformation in the SC, forming a long-acting drug reservoir in the epidermal layer. Furthermore, in the imiquimod-induced psoriasis mouse model, MAP-F127/Cur demonstrated a significantly enhanced therapeutic effect.

Conclusion: : This study not only provides a new delivery strategy for Cur in the treatment of psoriasis, but also offers an important reference for designing transdermal delivery systems for other dermatological drugs.

Keywords: curcumin, mussel adhesive protein, pluronic F127 micelles, topical delivery, psoriasis

Introduction

Psoriasis is a long-term inflammatory dermatosis that exerts a substantial influence on the physical and psychological well-being of the affected people.[1] The typical histopathological feature of psoriasis is epidermal hyperplasia accompanied by extensive lymphocyte and neutrophil infiltration.[2] Patients usually have clinical symptoms such as erythema, scales shedding and epidermal thickening. Local administration of pharmaceutical preparations to skin lesions can effectively alleviate the symptoms of psoriasis, which has become one of the most widely used treatment methods.[3] Compared with the systemic administration route, topical administration can reduce the absorption rate of the drug

Received: 17 September 2025
Accepted: 5 December 2025
Published: 9 December 2025

throughout the body, thereby improving the therapeutic effect.[4] However, owing to the formidable barrier properties of the SC and the difficulty of controlling the dynamic behavior of drugs in the skin, it is challenging for pharmaceuticals to achieve effective percutaneous permeation and skin targeting, which leads to the reduction of the utilization rate of topical drugs and ultimately affects the clinical treatment effect.[5]

Curcumin (Cur), a natural bioactive compound extracted from the rhizome of turmeric, has garnered considerable interest in the medical community due to its demonstrated efficacy in topical psoriasis therapy.[6] However, Cur has drawbacks such as poor water solubility and chemical stability, as well as low skin permeability, which seriously restrict the manifestation of its clinical efficacy.[7] In response to these deficiencies, various nano-delivery systems, such as polymer micelles, nanogels, and nano-emulsions, have been developed to improve the pharmacological activity of Cur in topical drug delivery.[8]

Polymeric micelles possess the benefits of straightforward preparation, low critical micelle concentration (CMC) and good stability, which can effectively encapsulate hydrophobic drug molecules and significantly improve their skin permeability.[9] Polymer micelles can be absorbed into the skin by transcellular transport, intercellular penetration, and hair follicle appendages.[10] In addition, polymer micelles can effectively overcome the SC barrier due to their nanoscale size.[11] Therefore, polymeric micelles are regarded as an ideal carrier system for topical drug delivery and topical disease management in the field of nanomedicine. However, polymer micelles still have the limitation of insufficient skin-targeted accumulation for drugs. To address this challenge, functional treatment of micelle surface has been applied to enhance the ability of skin-targeted drug delivery.

Pluronic F127 (F127) is a nonionic block copolymer with exceptional biocompatibility that allows for chemical modification to fabricate functional drug delivery systems, which improve the therapeutic effects of drugs by strengthening the tissue adhesiveness or targeting abilities.[12] The mussel adhesive protein (MAP) secreted by the byssus gland of Marine mussels is a macromolecular protein rich in 3, 4-dihydroxyphenylalanine (DOPA), and the catechol group of DOPA endows MAP with extremely strong biological adhesion ability through chelation and hydrogen bonding with the substrate.[13] In addition, MAP molecules can achieve firm and stable cell adhesion via electrostatic interactions between their positively charged amino acids and negatively charged cells, as well as hydrophobic bonding between their hydrophobic groups and the phospholipid layers of cell membranes.[14,15] These unique properties make MAP highly valuable for constructing functional nano-delivery systems. For instance, mussel-protein-based nanoparticles have been developed as sprayable adhesive nanotherapeutics for highly efficient locoregional cancer therapy, which demonstrates the great potential of MAP in drug delivery systems.[16] Therefore, MAP is expected to significantly improve the drug delivery efficiency for localized psoriasis treatment.

In the present research, a carrier material derived from MAP-functionalized Pluronic F127 was designed and developed, and the MAP-modified Pluronic F127 micelles loaded with Cur (MAP-F127/Cur) were constructed, aiming to promote the cutaneous absorption of Cur and enhance the topical therapeutic efficacy in psoriasis (Figure 1). The physicochemical characterization of MAP-F127/Cur was performed and the skin permeation and retention capabilities of MAP-F127/Cur were verified through in vitro experiments. Furthermore, imiquimod (IMQ)-induced psoriasis mouse model was employed to assess the in vivo efficacy of the MAP-F127/Cur, which confirmed that the MAP-F127/Cur could significantly enhance the local therapeutic effect of Cur, thereby provides an important reference for developing an efficient nanocarrier in the management of dermatological disorders.

Materials and Methods

Materials

Pluronic F127 was purchased from BASF Corporation (Shanghai, China). Mussel adhesion protein (100 kDa) was purchased from USUN Biochemical Technology Co., Ltd. (Jiangyin, China). Curcumin was purchased from Shandong Yatu Biotechnology Co., Ltd. (Jinan, China). 4-dimethylaminopyridine (DMAP), succinic anhydride, 1- (3-dimethylaminopypropyl) −3-ethylcarbodiimide hydrochloride (EDC), and N-hydroxysuccinimide (NHS) were purchased from Aladin (Shanghai, China). Pyrene was purchased from Macklin (Shanghai, China). Imiquimod Ointment (5%, w/w) was bought from Mingxin Pharmaceutical Co., Ltd. (Chengdu, China). Clobetasol propionate cream (0.02%, w/w) was

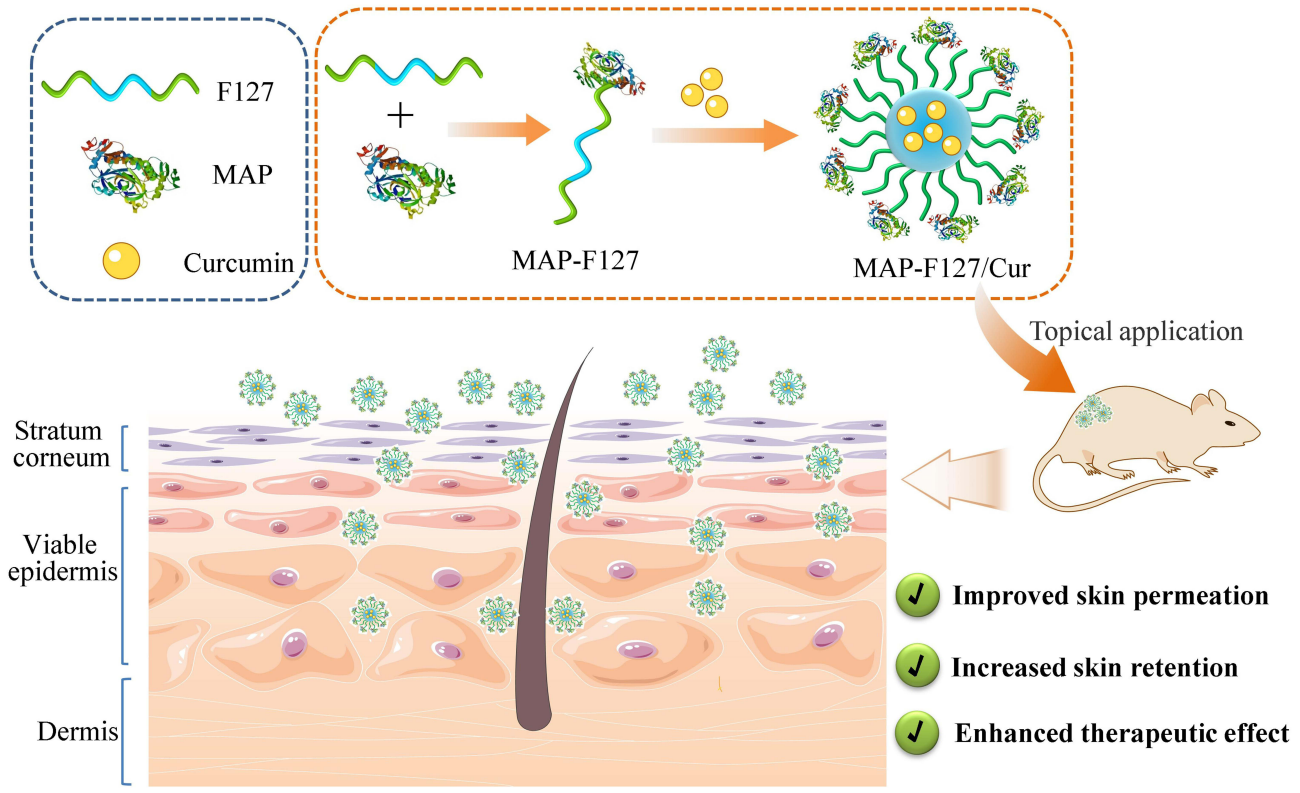

Figure 1 Schematic illustration of the MAP-F127/Cur for enhanced topical delivery of Cur, including improved skin permeation, increased skin retention, and enhanced therapeutic effect.

purchased from Guangdong Resources Shunfeng Pharmaceutical Co., Ltd. (Foshan, China). The One-month-old Bama miniature porcine skin was supplied by Linxi County Jingde Agricultural Products Sales Co., Ltd. (Jingde, China).

Synthesis and Characterization of MAP-F127

Synthesis and Structural Confirmation of MAP-F127

To provide carboxyl active functional groups for binding to MAP, carboxylated Pluronic F127 (F127-COOH) was synthesized.[17] Pluronic F127 (5 g) was dissolved in 25 mL of methylene chloride. Subsequently, DMAP (51 mg), succinic anhydride (386 mg) and triethylamine (78 mg) were added and stirred continuously at ambient temperature for 48 h. The reaction mixture was first filtered through a microporous membrane filter, followed by precipitation with cold diethyl ether. The obtained precipitate was redissolved in ethanol, dialyzed, and freeze-dried to obtain F127-COOH. F127-COOH (2.6 g) was activated using EDC (0.12 g) and NHS (0.07 g) in 25 mL of MES buffer (pH=5.5) at 37 °C for 30 min, while MAP was dissolved in 12 mL of MES buffer, and then MAP solution was added drop by drop to the activated F127-COOH solution with constant stirring. The coupling process was completed by stirring for 6 h at 37 °C. The final reaction product was purified by dialysis and freeze-dried to obtain MAP-F127. The chemical structure of MAP-F127 was identified by Fourier transform infrared (FTIR) spectroscopy (Nicolet iS-5, Thermo, USA) and ^{1}H nuclear magnetic resonance (^{1}H NMR) spectrometer (Avance II 400, Bruker, Karlsruhe, Germany).

Measurement of Critical Micelle Concentration (CMC)

The CMC of MAP-F127 was measured using pyrene fluorescence probe methodology.[18] Firstly, six equal volumes of pyrene solution (5×10^{-7} M) were placed in darkness for 24 h to completely volatilize the methanol. Subsequently, 10 mL of MAP-F127 aqueous solutions with a series of concentrations (0.01−2.5 g/L) were added respectively, sonicated for 10 min, and then equilibrated in darkness for 24 h. The samples were detected using the fluorescence spectrophotometer (F-7000, Tokyo, Japan). The excitation wavelength was set to 334 nm, and the fluorescence intensity values (I_{372} and I_3

https://doi.org/10.2147/IJN.S563465

$_{83}$) at 372 nm and 383 nm were recorded respectively. The CMC value was determined by plotting the relationship curve between the ratio of I_{383}/I_{372} and the logarithm of MAP-F127 concentration (Log C).

Formulation and Characterization of MAP-F127/Cur

Formulation of MAP-F127/Cur

MAP-F127/Cur was prepared using the thin-film hydration method. Cur (5 mg) and MAP-F127 (50 mg) were dissolved in 10 mL of absolute ethanol, and the solvent was evaporated using rotary evaporation at 45 °C, resulting in a thin film formation. Subsequently, hydration was performed at 60 °C for 30 min by adding 5 mL of deionized water, followed by ultrasonic treatment for 5 min to promote the self-assembly of the micelles. F127/Cur and blank micelles were prepared using the same process with a constant concentration of F127 polymer. The appearance and the Tyndall phenomenon of MAP-F127/Cur were visually inspected. The UV-Vis and fluorescence spectra of both MAP-F127/Cur and Cur solution (10 μg/mL) were further analyzed.

Entrapment Efficiency (EE) and Drug Loading (DL)

Free Cur in MAP-F127/Cur was separated using centrifugation at 3000 rpm for 30 min with an ultrafiltration tube (MWCO 30 kDa). Cur was dissolved in ethanol to prepare a series of standard solutions with concentrations ranging from 0.2 to 6.0 μg/mL. The absorbance was measured at 423 nm using a UV-vis spectrophotometer (TU-1810PC, Purkinje, China), and a standard curve was constructed to obtain the linear equation A= 0.1609C – 0.0042 (R^2=0.9978). The EE and DL were calculated using the following equation:

$$\mathrm{EE}(\%) = \text{Weight of encapsulated Cur}/\text{Weight of feeding Cur} \times 100\%$$

$$\mathrm{DL}(\%) = \text{Weight of encapsulated Cur}/\text{Weight of total MAP} - \mathrm{F127}/\mathrm{Cur} \times 100\%$$

Morphology, Particle Size and Zeta Potential

The morphology of the MAP-F127/Cur was examined by scanning electron microscopy (SEM) (Sigma500, Zeiss, Oberkochen, Germany). MAP-F127/Cur was diluted 100 times with deionized water, and an appropriate amount of the diluted formulation was applied onto a monocrystalline substrate and freeze-dried. The sample was gold-sputtered under vacuum conditions and then observed at an appropriate magnification. The particle size and zeta potential of MAP-F127/Cur were detected with a Zetasizer (ZS90, Malvern, UK) at 25 °C, at a fixed detection angle of 90°.

FTIR and XRD

The possible interactions of Cur in MAP-F127 micelles were investigated using a FTIR spectrometer (Nicolet iS5, Thermo, USA). The infrared spectra of the samples were recorded in transmission mode over the wavelength range of 400–4000 cm^{-1} with a spectral resolution of 4 cm^{-1}, and a total of 64 scans were performed. X-ray diffraction (XRD) analysis was performed using an X-ray diffractometer (D8 Advance, Bruker, Germany) to study the physicochemical changes of Cur in MAP-F127 micelles. XRD measurements were conducted using Cu−Kα radiation generated at 40 kV and 40 mA with a scanning range of 5−40° (2θ).

Short Term Stability

The short-term stability of MAP-F127/Cur was investigated in the dark at 4 °C and 25 °C on days 0, 1, 5, 7, and 14 after formulation. During storage, visual inspection was performed, and physicochemical characteristics of the micelles, including particle size, zeta potential, EE, and DL, were also evaluated.

In vitro Drug Release Study

The in vitro drug release study was conducted using the dialysis membrane method.[19] The release medium consisted of phosphate-buffered saline (PBS, pH 7.4) supplemented with 1% (v/v) Tween-80. Aliquots of 2 mL of MAP-F127/Cur, F127/Cur, or Cur ethanol solution were separately introduced into a dialysis tube (MWCO 35 kDa). The tube was sealed at both ends and immersed in 40 mL of preheated release medium. The experiment was conducted in a water bath

maintained at 37 ± 1°C with horizontal shaking at 50 rpm. At predetermined time intervals, 2 mL aliquots of release medium were withdrawn and immediately replaced with an equal volume of fresh preheated medium. Drug content in each sample was analyzed at 423 nm using UV-Vis spectrophotometry and cumulative drug release was calculated.

In vitro Skin Permeation and Retention Study

Quantification of Cur by HPLC

In the study of skin permeation and retention, the content of Cur was analyzed by means of a high-performance liquid chromatography (HPLC) technology equipped with a UV detector and a reversed-phase C18 chromatographic column (5 mm, 200×4.6 mm). The mobile phase was a mixture of acetonitrile and water (58:42, v/v) supplemented with 0.5% phosphoric acid, delivered at a flow rate of 1.0 mL/min. The column temperature was maintained at 30.0±0.2 °C, with each sample injected at a volume of 20 μL and signals monitored at 423 nm.

Skin Permeation Study

Skin permeation was investigated utilizing a Franz diffusion cell (RYJ-6B, Huanghai, China) consisting of a donor chamber and a recipient chamber.[20] The receptor chamber of the diffusion cell had a capacity of 6.5 mL and an effective membrane contact area of 2.8 cm^2. The porcine skin was fixed between the two chambers with the epidermis oriented towards the donor chamber. The PBS containing 1% Tween-80 (pH 7.4) was added to the receptor chamber and placed in a water bath (37±0.5 °C) with continuous agitation at a speed of 300 rpm. After equilibration for 20 min, 1 mL of Cur solution, F127/Cur and MAP-F127/Cur (equal to 0.2 mg of Cur) was respectively applied to the skin surface. At set time intervals, 1 mL of the receptor solution was removed from the receptor chamber and right away replaced with the same volume of fresh PBS. The content of the drug was measured using HPLC, and the cumulative permeation amount of Cur was computed.

Skin Retention Study

When the permeation experiment came to the end, skin samples were taken out of the Franz diffusion cells. The remaining formulation on the surface of skin was eliminated through careful rinsing with deionized water. These skin samples were then cut into small fragments and soaked in 2 mL of methanol. Following 24 h of storage at 4 °C, the samples were subjected to 30 min of ultrasonic treatment, and then centrifuged at 3000 rpm for 15 min to collect the supernatant. The quantity of Cur remaining in the skin was assessed using HPLC.

In vitro Skin Distribution Study

Porcine skin was treated with MAP-F127/Cur, F127/Cur and Cur solutions for 2 h and 8 h, respectively. The skin was taken out of the Franz diffusion cell and vertical slices with a thickness of 10 μm were prepared using a cryostat (CM1950, Leica, Germany). The skin slices were stained by DAPI and fluorescence images were obtained using a digital scanning system (Pannoramic MIDI, 3DHISTECH, Hungary) to examine the distribution of Cur within the skin.

Histological Observation

Porcine skin was mounted on Franz diffusion cells and exposed to physiological saline (control), F127/Cur and MAP-F127/Cur for 12 h, respectively. The skin samples were then removed, rinsed using physiological saline and placed in a 4% paraformaldehyde solution for fixation, followed by dehydration through a series of ethanol solutions with increasing concentrations. Subsequently, the samples were placed in xylene for transparent processing, embedded in paraffin, longitudinally sliced with pathological microtome (LEICA RM2235, Nussloch, Germany) at a thickness of 5 μm, stained using hematoxylin and eosin (HE), sealed with neutral gum, and histopathological alterations were examined with a digital scanner (3DHISTECH Ltd, Budapest, Hungary).

Interaction Mechanisms of MAP-F127/Cur with the Skin

SEM Analysis of Skin Surface

Porcine skin samples were exposed to physiological saline (control), Cur solution, F127/Cur and MAP-F127/Cur for 12 h in Franz diffusion cells, rinsed thoroughly with physiological saline and fixed with 4% paraformaldehyde at 4 °C for 24 h. Following fixation, skin samples were cleansed with physiological saline and subsequently freeze-dried with

a lyophilizer (SCIENTZ-18N, Xinzhi, China) for 48 h. The dried skin samples were fixed on aluminum stubs, coated with gold through spraying, and the skin surface was examined using SEM (Sigma 500, ZEISS, Germany).

DSC Analysis of Skin Thermotropic Properties

The effects of different formulations on the thermogenic properties of skin were analyzed via differential scanning calorimetry (DSC, Q2000, TA Instrument, USA). Porcine skin samples were treated in Franz diffusion cells with physiological saline (control), Cur solution, F127/Cur, and MAP-F127/Cur respectively for 12 h. Then the administration site of the skin was cleansed using physiological saline, freeze-dried for 48 h and cut into small pieces. About 8 mg of skin pieces were weighed and sealed in an aluminum crucible. DSC analysis was conducted by heating the temperature from 0 °C to 250 °C at a speed of 10 °C /min in a nitrogen environment.

FTIR Analysis of Skin Structure

Skin samples exposed to various formulations were processed according to the DSC analysis. An FTIR spectrometer (Nicolet iS5, Thermo, USA) was used to collect the infrared spectra of the skin samples. The process covered the wavenumber range from 400 to 4000 cm^{-1}, involving the combination of 64 scans at a resolution of 4 cm^{-1}, and all operations were carried out under ambient temperature.

Trans-Epidermal Water Loss (TEWL) Analysis

To study the impact of different formulations on the function of the skin barrier, measurement of TEWL was performed with a Tewameter® TM 300 (Courage & Khazaka, Germany). The porcine skin was fixed in the Franz diffusion cell and treated respectively with physiological saline (control), Cur solution, F127/Cur and MAP-F127/Cur for 12 h. Following treatment completion, the skin samples were removed, gently cleansed with physiological saline, blotted dry with filter paper, and subjected to TEWL evaluation with a probe at 10 min and 24 h.

Therapeutic Effect on Imiquimod-Induced Psoriasis in Mice

Female KM mice aged 6–8 weeks were randomly assigned to 6 groups: normal, model, Cur solution, F127/Cur, MAP-F127/Cur and clobetasol propionate (CP). Each group consisted of 6 mice. The dorsal area of the mice was shaved 24 h prior to the experiment. In addition to the normal group, imiquimod (IMQ) ointment (25 mg/cm^2) was applied daily on the back of the other groups to induce psoriasis-like lesions. Excluding the normal and model groups, the treatment groups were administered corresponding Cur formulations (0.2 mL/cm^2), and the positive control group was treated with CP cream (50 mg/cm^2). All treatments were carried out once a day.

The degree of skin inflammation was evaluated using the scoring methodology of Psoriasis Area and Severity Index (PASI). At the termination of the experiment, the mice were euthanized. Skin samples were collected and fixed with 4.0% paraformaldehyde. The skin samples were sectioned, stained with HE, and visualized using the scanner (KF-PRX-040, KFBIO, china) to analyze the histological changes related to psoriasis. The spleen index was computed using the following equation:

$$\text{Spleen index} = \text{Spleen weight (mg)}/\text{Body weight of the mouse (g)}$$

Statistical Analysis

Experiments were performed with at least three independent biological replicates for each group. All measurements are reported as mean ± SD. Statistical comparisons were performed using an independent samples *t*-test for two-group comparisons and a one-way ANOVA with post-hoc Tukey's tests for multi-group comparisons. Values with statistical significance were set at $p < 0.05$.

Results and Discussion

Characterization of MAP-F127

Characterization by FTIR and ^1H NMR

Figure 2A shows FTIR spectra of F127, F127-COOH, MAP and MAP-F127. In the FTIR spectrum of F127, the absorption bands at 1101 and 1278 cm^{-1} were attributed to the C−O−C stretching vibration of aliphatic ether groups and

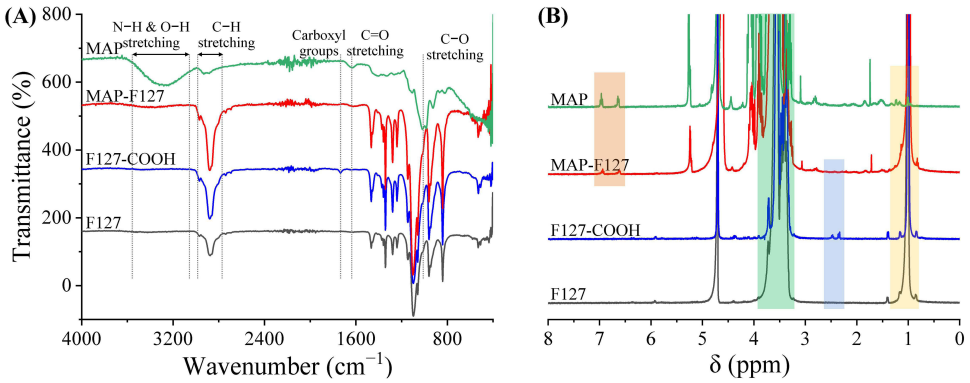

Figure 2 (**A**) FTIR spectra and (**B**) ^{1}H NMR spectra of F127, F127-COOH, MAP and MAP-F127.

$-CH_2$ twisting vibration,[21] respectively. Following the carboxylation of F127 using succinic anhydride, a new peak assigned to the stretching vibration of carboxyl group (−COOH) was detected at 1735 cm^{-1}, which confirmed the successful carboxylation of F127.[22] The spectrum of MAP showed the characteristic absorption bands belonging to amide bonds and 3,4-dihydroxyphenylalanine (DOPA) groups. The absorption band occurring within the range of 1700 −1600 cm^{-1} was primarily ascribed to the stretching vibration of the carbonyl group (C=O). The broad absorption peak spanning from 3600 to 3100 cm^{-1} was attributed to the stretching vibrations of N−H and O−H bonds. Additionally, the peaks in the range from3000 to 2800 cm^{-1} corresponded to C−H stretching vibrations, whereas the absorption band at 1018 cm^{-1} was ascribed to the C−O stretching vibration specific to the DOPA groups.[23] After conjugation of F127-COOH and MAP, a distinct characteristic peak emerged at 1620 cm^{-1}, which was ascribed to the C=O stretching vibration of the amide bond formed between the carboxyl group of F127-COOH and the primary amine group of MAP.[24] Furthermore, the disappearance of the peak at 1735 cm^{-1} related to the carboxyl groups also supported the successful conjugation of MAP to F127-COOH.

To further confirm the conjugation of MAP and F127-COOH, ^{1}H NMR spectroscopy was adopted, with the results presented in Figure 2B. For the F127-COOH, the peaks at 3.2–3.8 and 1.1 ppm corresponded to the ethylene proton (CH_2-CH_2) of poly(ethylene oxide) (PEO) and the methyl protons ($OCH_2CH(CH)_3O$) of poly(propylene oxide) (PPO), respectively. The weak resonance signals appeared at 2.5 ppm assigned to the methylene protons (CH_2CH_2COOH) of the succinic groups, provided additional evidence that carboxyl groups had successfully conjugated to the terminal hydroxyl groups of F127.[25] Based on the peak areas of the methyl protons at 1.1 ppm and methylene protons at 2.5 ppm in the spectrum of F127-COOH, approximately 68% of the hydroxyl groups in F127 were found to be conjugated with carboxyl groups. The spectrum of MAP presented the characteristic peaks of protons from the DOPA groups at 6.6–7.0 ppm.[26] The spectrum of the MAP-F127 contained both the major peaks of F127 and the characteristic peaks of MAP, which further confirmed the successful conjugation of MAP to F127-COOH by EDC/NHS chemistry, as shown in Figure 3A.

CMC of MAP-F127

Figure 3B shows the intensity ratio of I_{372}/I_{383} with the logarithmic concentration of the MAP-F127 aqueous solution. At the concentration below the CMC, MAP-F127 exhibited nearly constant I_{372}/I_{383} values. However, when the concentration exceeded CMC, the ratio decreased significantly, indicating that the pyrene molecules migrated from aqueous domains to hydrophobic microenvironments. Meanwhile, MAP-F127 formed micellar structure through self-aggregation. The CMC value was obtained by fitting the linear trend line of the low and high concentration interval and taking the abscise of the intersection point. The results showed that the CMC of MAP-F127 at 25 °C was 0.125 mg/mL, which was dramatically lower than the reference range of F127 (1–7 g/L),[27] indicating that MAP-F127 had a stronger self-assembly ability, and its micellar structure was more stable due to the steric hindrances effect of the MAP and the enhanced intermolecular forces. This stability is very beneficial for maintaining the micellar structure during transdermal delivery.[28]

https://doi.org/10.2147/IJN.S563465

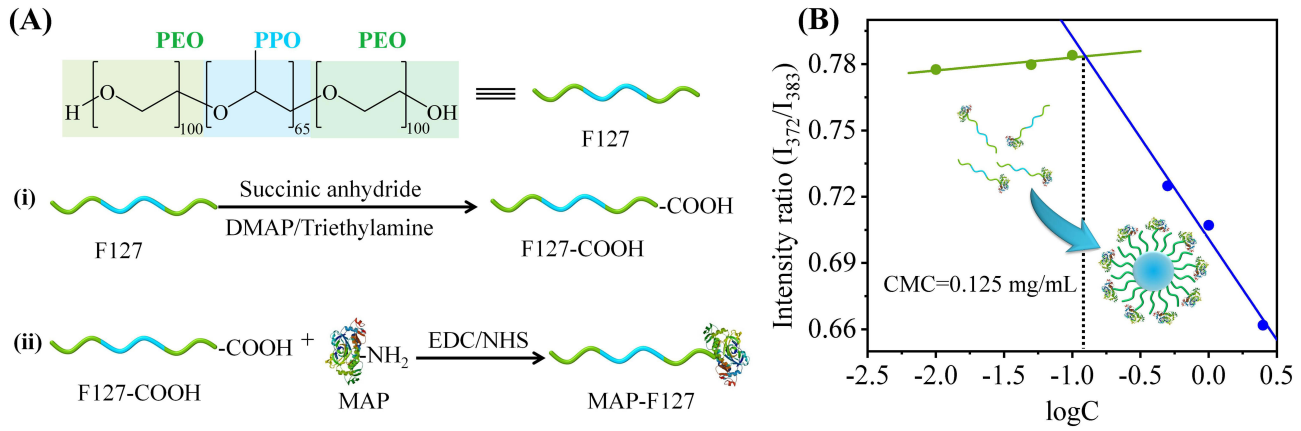

Figure 3 (**A**) Diagrammatic scheme for synthesis of MAP-F127. (**B**) Variation of fluorescence intensity ratio (I_{372}/I_{383}) with logarithmic concentration of MAP-F127.

Preparation and Characterization of MAP-F127/Cur

This investigation employed MAP-F127 micellar encapsulation to enhance the therapeutic efficacy of curcumin (Cur) in the treatment of psoriasis. Drug encapsulation was achieved through hydrophobic interactions between drug molecules and the lipophilic segments of the amphiphilic polymer. The molecular structure of Cur contains a chromophore composed of an aromatic π-electron system, and its spectral characteristics can be used to analyze intermolecular interactions. UV-Vis absorption spectroscopy results showed (Figure 4A) that the maximum absorption peak of MAP-F127/Cur was located at 421 nm, while the peak of free Cur appeared at 425 nm. This blue shift phenomenon arises from the overlap of π-electron clouds, which is caused by the elevated local concentration of Cur and the enhanced interactions between drug molecules.[29] More striking evidence was provided by fluorescence spectroscopy (Figure 4B). In comparison with non-encapsulated Cur of identical concentration, the fluorescence intensity of Cur loaded into micelles decreased significantly, which was attributed to the self-quenching effect triggered by the increased local concentration of Cur within the hydrophobic core of the micelles,[30] indicating effective encapsulation of Cur molecules.

EE and DL are two key parameters to evaluate the performance of polymer micelles, which not only reflect the binding ability of the carrier to the drug, but also directly affect the delivery efficiency and sustained release characteristics of the drug.[31] The EE and DL of MAP-F127/Cur were 93.06±1.47% and 8.51±0.14%, respectively, showing excellent drug-loading performance, which might be attributed to the substantial hydrophobic domains in the copolymer structure of F127 copolymer structure. Research has demonstrated that hydrophobic drugs are primarily incorporated within micellar cores via multiple non-covalent forces, including hydrophobic effects, hydrogen bonding, and van der Waals interactions.[32] The high drug-loading efficiency of MAP-F127/Cur will be beneficial for improving the topical bioavailability of drugs.

MAP-F127/Cur appeared as an orange-yellow transparent liquid. Upon laser irradiation, the sample exhibited a distinct light scattering path (Figure 4C), demonstrating the Tyndall effect, which confirmed the self-assembly of MAP-F127 into colloidal nanoparticles with dimensions smaller than visible light wavelengths in aqueous medium.[33] The SEM image of MAP-F127/Cur is shown in Figure 4D. The MAP-F127/Cur exhibited uniform spherical morphology with homogeneous distribution, displaying an average diameter of approximately 30 nm. Figure 4E illustrates the size distribution of blank micelles and drug-encapsulated micelles. The results demonstrated that all samples exhibited monomodal size distributions with polydispersity index (PDI) values below 0.3, which was helpful to maintain the stability of micelles. Comparative analysis of Pluronic F127 micelles before and after drug encapsulation revealed a micellar size increase from 26.38 nm to 33.06 nm. Similarly, MAP-F127 micelles showed comparable behavior, with average diameter increasing from 34.99 nm for blank micelles to 47.50 nm after drug loading. This size expansion primarily resulted from the incorporation of drug molecules into the hydrophobic core of the micelles, leading to structural swelling.[34] Moreover, the size of MAP-modified micelles was larger than that of unmodified micelles, which might be related to the MAP surface coating. It is worth noting that the particle size determined via dynamic light scattering (DLS) was smaller than that measured using SEM. This

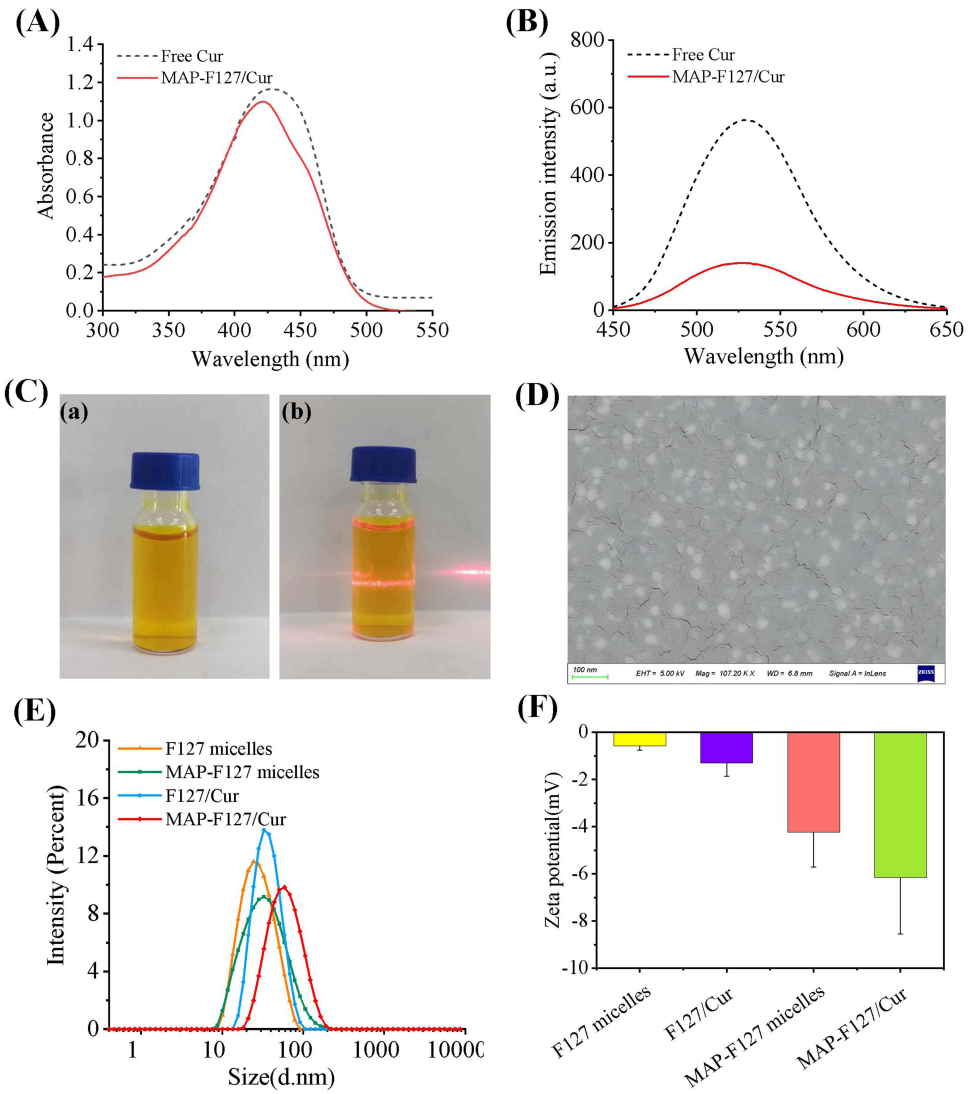

Figure 4 (**A**) UV-Vis and (**B**) fluorescence spectra of Cur solution and MAP-F127/Cur at 10 μg/mL. (**C**) Appearance (a) and Tyndall phenomenon (b) of the MAP-F127/Cur. (**D**) SEM image of MAP-F127/Cur. (**E**) Size distribution and (**F**) zeta potential of F127 micelles, MAP-F127 micelles, F127/Cur and MAP-F127/Cur.

difference might be attributed to the fact that samples observed via SEM were dried, whereas micelles were in a hydrated and swollen state when detected by DLS.[35] Nanoparticles with size smaller than 300 nm had been reported to be suitable for skin topical drug delivery.[36] Therefore, the small size of MAP-F127/Cur is conducive to its permeation into the SC and deposition in the skin. The zeta potential showed that all the micelles are negatively charged (Figure 4F). The mean zeta potential of F127 blank micelles and F127/Cur was −0.57 mV and −1.30 mV, respectively. This low absolute zeta potential value is attributed to the nonionic nature of Pluronic polymers. The zeta potential of MAP-F127 blank micelle and MAP-F127/Cur was −4.24 mV and −6.16 mV, respectively. MAP-F127/Cur carried more negative charges, which might be related to the carboxyl groups in MAP-F127 molecules. The surface charge characteristics of nanoparticles may affect their skin permeability and retention. Owing to the negative charge present on the skin surface, negatively charged nanoparticles are more likely to be deposited in the skin than positively charged nanoparticles, which could be accounted for by the electrostatic repulsion between negatively charged nanoparticles and skin lipids disrupting the epidermal tight junction structure, thereby enhancing the drug delivery to the skin.[37]

https://doi.org/10.2147/IJN.S563465

FTIR and XRD

FTIR Analysis

FTIR can be used to analyze the interaction between drugs and polymers, and provide further supporting evidence for drug encapsulation.[38] Figure 5A shows the FTIR spectra of pure Cur, physical mixture of Cur and MAP-F127, freeze-dried MAP-F127 blank micelles and MAP-F127/Cur. The spectrum of Cur showed that the sharp peak at 3510 cm^{-1} was ascribed to the stretching vibration of hydroxyl group (–OH). The characteristic peaks at 1626 cm^{-1} and 1506 cm^{-1} corresponded respectively to the stretching vibrations of the carbonyl group (–C=O) and the aromatic ring (C=C). Furthermore, the peak at 1024 cm^{-1} originated from the asymmetric stretching vibration of the ether linkage (C−O−C).[39] The spectrum of blank micelles exhibited a peak at 2883 cm^{-1}, which can be ascribed to the C–H stretching vibration of MAP-F127. In the spectrum of the physical mixture, the primary characteristic peaks of both Cur and MAP-F127 were preserved, with no shifts in their positions. However, when Cur was encapsulated in MAP-F127 micelles, the spectral features at 3510 cm^{-1}, 1626 cm^{-1}, and 1024 cm^{-1} disappeared completely, and the intensity of the C=C vibration peak at 1506 cm^{-1} was significantly reduced. These spectral changes suggest that there may be hydrogen bonds or dipole interactions between Cur and MAP-F127. The interaction between Cur and MAP-F127 further confirms that the drug was effectively encapsulated in the polymer micelles, and this interaction also helps MAP-F127/Cur achieve sustained drug release.[40]

XRD Analysis

The XRD diffractograms of pure Cur, the physical mixture of Cur and MAP-F127, blank MAP-F127 micelles, and MAP-F127/Cur are presented in Figure 5B. The diffractogram of Cur exhibited intense diffraction peaks at 8.88°, 17.32°, 19.48°, and 25.61°, which were mainly attributed to its crystalline nature.[41] After Cur was physically mixed with MAP-F127, the strength of the typical diffraction peaks of Cur was significantly reduced as a result of being diluted with MAP-F127. The diffraction pattern of MAP-F127/Cur was similar to that of blank micelles, but significantly different from that of Cur. In the diffraction pattern of MAP-F127/Cur, the diffraction peaks corresponding to Cur vanished entirely, suggesting that Cur transitioned from a crystalline structure to an amorphous state.[42] This transformation of the physical state might be due to the intermolecular interaction between the Cur and MAP-F127. The complete vanishing of the crystalline diffraction patterns of the Cur further confirms the successful drug encapsulation.

Stability Evaluation

The stability of MAP-F127/Cur under different storage conditions was evaluated over a two-week period, with key parameters including encapsulation efficiency (EE), drug loading (DL), particle size, and zeta potential being monitored. The results showed that after 14 days of storage at 4°C, the EE of MAP-F127/Cur decreased by 7.68% and the DL by 0.64% compared to the initial (day 0) values. In contrast, at 25°C, the EE decreased by 21.19% and the DL by 1.82%, along with noticeable drug leakage (Figure 6A). Particle size analysis revealed that the initial diameter of MAP-F127/Cur was 46.9 nm. After 14 days at 4°C, it increased only slightly to 56.0 nm, with the PDI remaining below 0.2 (Figure 6B),

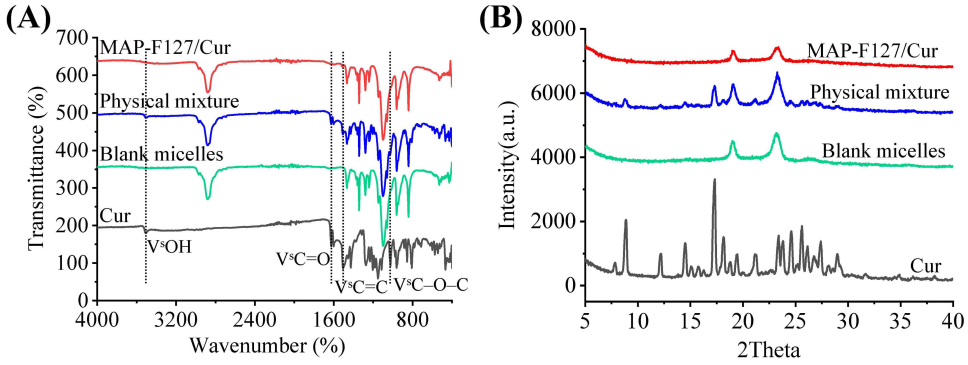

Figure 5 (**A**) FTIR spectra and (**B**) XRD diffractograms of MAP-F127/Cur, physical mixture of Cur and MAP-F127, blank MAP-F127 micelles and pure Cur.

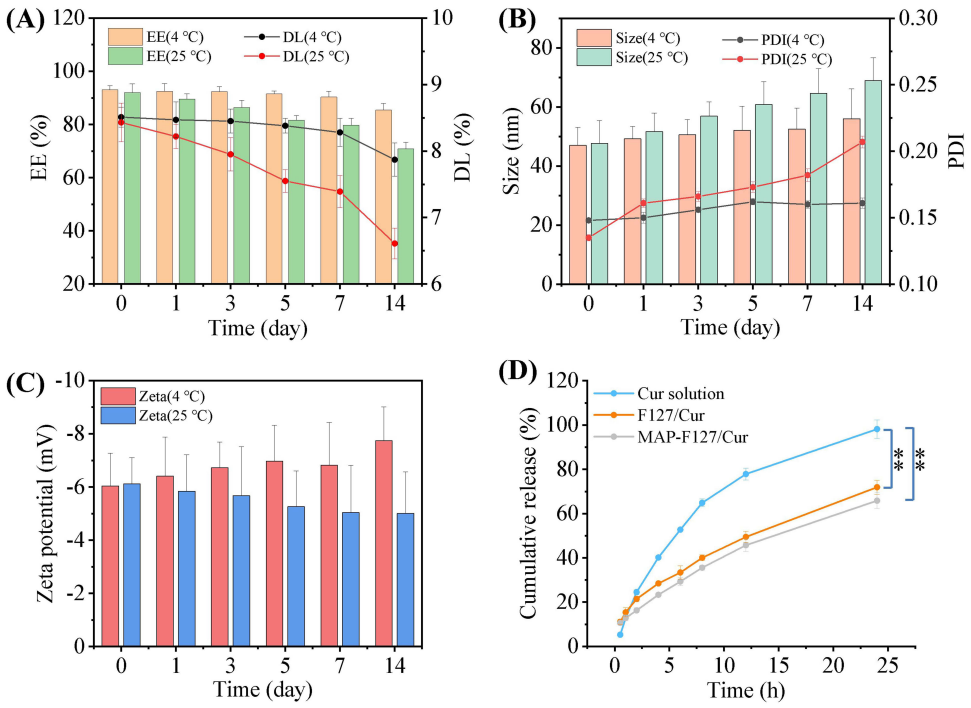

Figure 6 The stability of MAP-F127/Cur at 4 °C by (**A**) EE and DL, (**B**) size and PDI and (**C**) zeta potential. (**D**) The in vitro release of Cur from Cur solution, F127/Cur, and MAP-F127/Cur (n=3; $^{**}p < 0.01$).

indicating a homogeneous particle distribution. In comparison, storage at 25°C for the same period led to an increase in particle size from 47.7 nm to 68.95 nm, and the PDI rose from 0.14 to 0.21, suggesting possible particle aggregation in MAP-F127/Cur. Zeta potential measurements showed that after storage at 4°C, the absolute value increased from 6.04 mV to 7.74 mV, while it decreased from 6.12 mV to 5.01 mV at 25°C (Figure 6C). Therefore, MAP-F127/Cur demonstrated superior stability at 4°C compared to 25°C, indicating that refrigerated storage is more suitable for this formulation. However, as these findings are based on short-term data, a comprehensive long-term stability study is necessary to fully validate the shelf-life and support future translational development.

Drug Release Studies

The drug release characteristics of MAP-F127/Cur and F127/Cur within 24 h were investigated and compared with Cur solution. The Cur solution exhibited rapid release and was completely released within 24 h (Figure 6D), while MAP-F127/Cur and F127/Cur showed a significant sustained release. The cumulative drug release of MAP-F127/Cur and F127/Cur at 24 h were 65.85±3.62% and 71.92±3.16%, respectively, which were significantly lower compared with the Cur solution ($p < 0.01$). Through fitting analysis of the kinetics model, it was found that the Korsmeyer-Peppas model could most accurately describe the drug release behavior of MAP-F127/Cur (R^2=0.9991). The release index (n) was 0.48, suggesting that the drug release process of the formulation mainly follows the Fick diffusion mechanism, meaning that drug release is primarily driven by the concentration gradient.[43] For topical drug delivery, this implies that the drug may be released at a relatively stable and slow rate, which helps maintain a steady drug concentration at the lesion site, thereby prolonging the duration of action and reducing the frequency of administration[44] The sustained release of MAP-F127/Cur can be explained from two aspects. First, the three-dimensional network structure formed by polymer micelles can effectively hinder the free diffusion of drug molecules, significantly extending the pathway of the drug release.[45] Second, the strong interaction between drug molecules and the hydrophobic core of micelles acts as a barrier that retards drug release kinetics.[46] In the practical application of topical drug delivery, such sustained release is particularly important. It not only ensures that the drug can permeate smoothly into the deep skin and achieve continuous release but also effectively prevents the drug from being prematurely released on the SC surface, thereby avoiding failure to

https://doi.org/10.2147/IJN.S563465

reach the deep skin.[47] Additionally, the continuous drug release property helps maintain stable therapeutic effects and improves patient compliance by reducing the frequency of administration.

Skin Permeation and Retention Studies

Cur possesses notable anti-inflammatory and antioxidant capabilities, making it a commonly employed therapeutic agent for multiple dermatological conditions, particularly inflammatory disorders including psoriasis and atopic dermatitis. For topical treatments to be most effective, it is crucial to improve cutaneous drug retention while minimizing systemic uptake. Due to the high degree of similarity between porcine and human skin in both histological structure and physiological characteristics, porcine skin was chosen as the experimental model for this investigation.[48] The skin permeation behavior of MAP-F127/Cur was evaluated using the Franz diffusion technique. At the 12 h timepoint post-administration, the permeation amounts of Cur were 0.05±0.02 μg/cm^2, 0.17±0.01 μg/cm^2, and 0.07±0.02 μg/cm^2 for the Cur solution, F127/Cur, and MAP-F127/Cur, respectively (Figure 7A). The total amount of Cur that had permeated from MAP-F127/Cur was markedly smaller when compared with that in the F127/Cur group ($p < 0.01$), which suggests that MAP-F127 can effectively reduce the systemic absorption of drugs, thus reducing the occurrence of systemic adverse reactions.

The skin retention experiment aims to examine the drug accumulation ability of different preparations in the skin, which is crucial for ensuring that the drugs achieve the expected therapeutic effect. At 12 h post-application, the amount of Cur retained in the skin for the Cur solution, F127/Cur, and MAP-F127/Cur was 0.12±0.05 μg/cm^2, 0.28±0.05 μg/cm^2, and 0.61±0.08 μg/cm^2, respectively (Figure 7B). The amount of Cur retained in the skin for MAP-F127/Cur was found to be notably higher than that observed in both the Cur solution ($p < 0.001$) and F127/Cur ($p < 0.01$), demonstrating the best skin accumulation performance, the excellent skin retention of MAP-F127/Cur might be predominantly dependent on the bio-adhesion of MAP. The dopamine groups in the MAP structure can form strong adhesion to skin tissue through multiple interactions, including hydrogen bonds, covalent bonds, and cation-π/π-π interactions, thereby significantly improving the drug retention in the skin.[49–51] Meanwhile, the drug is distributed within the spherical structure of the micelles, and its slow-release characteristic helps in establishing a steady drug depot in the skin.[12] The research also found that polymer micelles can enhance the drug retention through the pathway of hair follicle, and their small hydrodynamic diameter is conducive to increasing the contact area with the skin, thereby promoting the diffusion and cutaneous accumulation.[52] Compared with conventional nanocarriers commonly employed in skin delivery research, the developed MAP-F127/Cur demonstrates superior performance in terms of skin retention. Previous studies have shown that the skin retention of topical Cur-loaded nanogels or liposomes is only 1–3 times that of Cur solutions, whereas the MAP-F127/Cur formulation achieves a retention approximately 5 times greater than that of Cur solutions.[36,53] Therefore, by leveraging the bio-adhesion of MAP, the MAP-F127/Cur system offers a unique delivery strategy that achieves superior skin retention and localized bioavailability compared to conventional nanocarriers. This enhanced drug availability within the skin is particularly advantageous for obtaining potent and prolonged pharmacological effects.

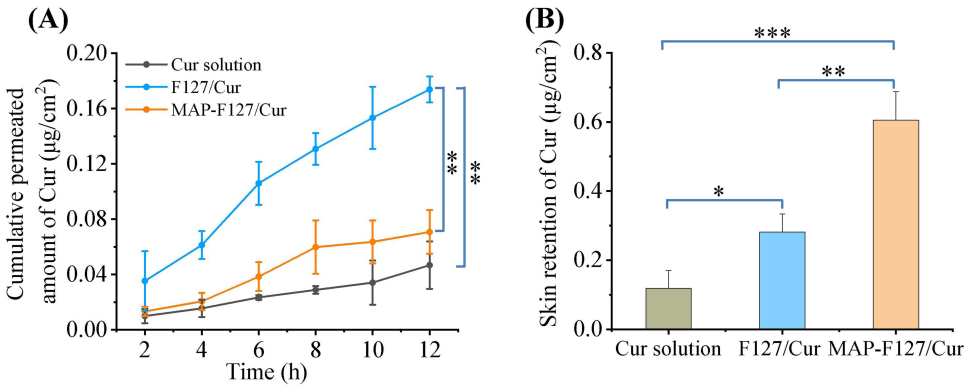

Figure 7 (**A**) In vitro skin permeation and (**B**) drug retention of Cur solution, F127/Cur, and MAP-F127/Cur in porcine skin (n=3; *$p < 0.05$, **$p < 0.01$, ***$p < 0.001$).

Visualization of Fluorescence Biodistribution

To investigate the skin localization and permeation pathways of the formulation, Cur solution, F127/Cur, and MAP-F127 /Cur were applied to porcine skin for 2 h and 8 h. Subsequently, the skin distribution of various formulations was observed. Figure 8A shows fluorescence images from two fluorescence emission measurements of the same skin section area (emission from DAPI-stained nuclei in the blue range and emission from Cur-loaded formulations in the green range). After treating the skin with different formulations for 2 h, only faint fluorescent signals were found in the SC of skin treated with the Cur solution, reflecting the poor skin permeation ability of Cur molecules. Skin treated with both F127/Cur and MAP-F127/Cur showed strong green fluorescence in the SC, indicating that micellar formulations can effectively promote drug permeation. At 8 h after administration, skin treated with F127/Cur exhibited widespread green fluorescent signals in both the SC and dermis, indicating that F127/Cur can promote the deep skin permeation of the drug. In contrast, when the skin was subjected to MAP-F127/Cur treatment, the green fluorescence was mostly restricted to the epidermis, and only weak signals were detected in the dermis. Quantitative analysis of fluorescence images

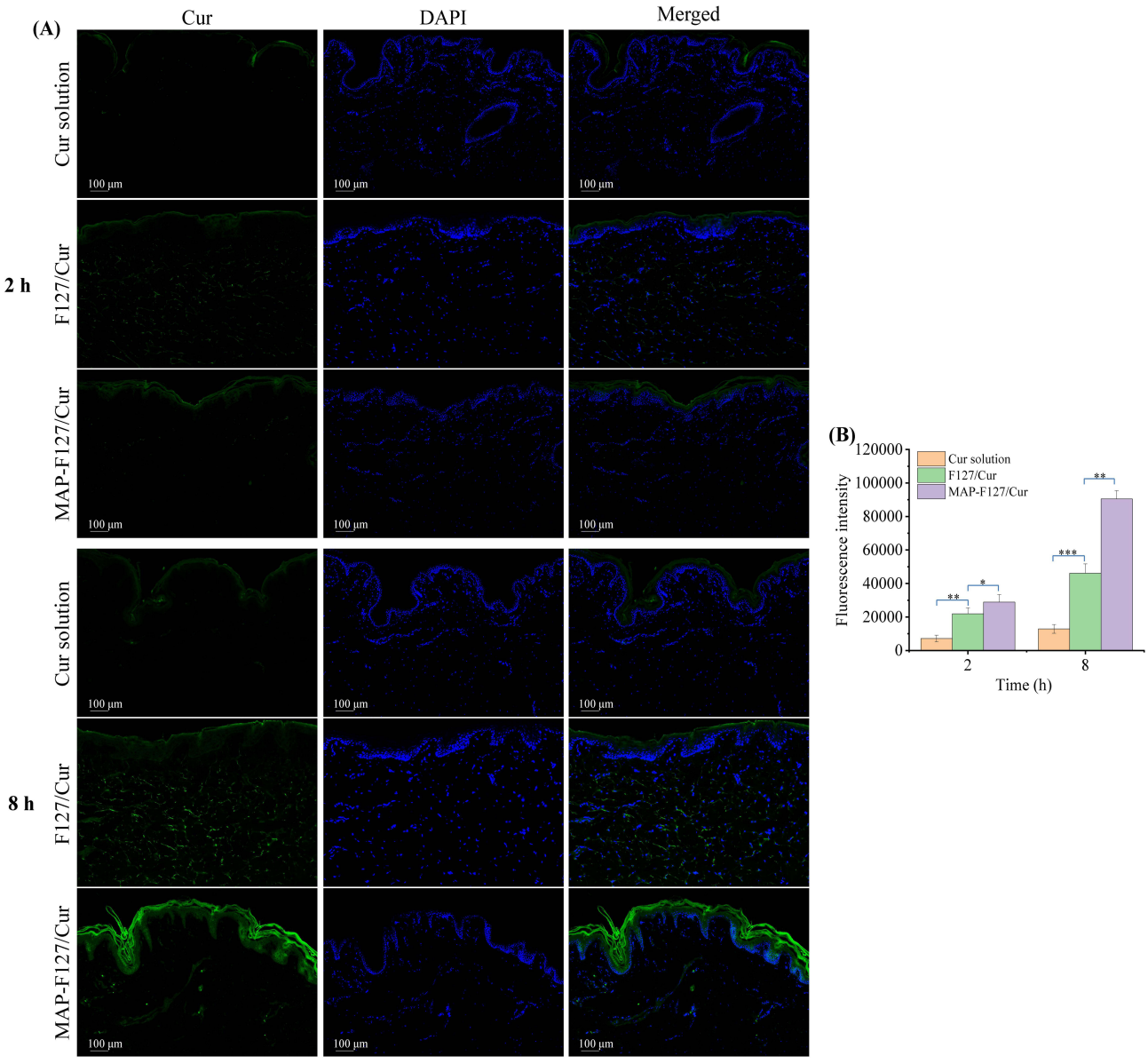

Figure 8 (**A**) Fluorescence images of the longitudinal sections of porcine skin samples treated with Cur solution, F127/Cur, and MAP-F127/Cur at 2 h and 8 h. (**B**) Fluorescence intensity of Cur after incubation with Cur formulation for 2 h and 8 h (n=3; *$p < 0.05$, **$p < 0.01$, ***$p < 0.001$).

https://doi.org/10.2147/IJN.S563465

revealed that the Cur signal intensity in the MAP-F127/Cur group was significantly stronger than that in the F127/Cur group ($p < 0.01$), particularly in the epidermal layer (Figure 8B). This indicates that MAP-F127/Cur can penetrate the SC and selectively accumulate in the epidermis to form drug reservoirs. This selective accumulation may be related to the tight adhesion of dopamine and lysine groups in the MAP structure to epidermal cells. These findings demonstrate that MAP-F127/Cur can improve the epidermal targeting of the drug, which would help reduce potential drug-related adverse effects associated with circulating distribution.[54] Furthermore, skin treated with MAP-F127/Cur also showed green fluorescence in the hair follicles. Quantitative fluorescence analysis revealed that the fluorescence intensity within hair follicles was 0.58 times that in the interfollicular skin, indicating that the skin permeation of MAP-F127/Cur occurs not only through the SC but also through hair follicles. It has been previously reported that the hair follicle route serves as a major pathway for nanoparticle permeation, largely attributable to the relatively large openings of hair follicle.[55] Therefore, MAP-F127/Cur can also be delivered targeting hair follicles, and their accumulation, deposition, and subsequent drug release can provide a more durable and effective local therapeutic effect.[56]

Histological Examination of the Skin

Microscopic images of porcine skin slices stained with HE following the application of different formulations are present in Figure 9. Visually, skin samples exposed to physiological saline or Cur solution maintained an intact structure with a compact SC, which was evenly distributed as strips over the viable epidermis (Figure 9A and B). In sharp contrast, the skin treated with F127/Cur and MAP-F127/Cur exhibited swelling, and the SC became loose, separated, and increased in thickness, which indicates that micellar formulations are capable of impairing the barrier capacity of the SC and enhancing drug permeation (Figure 9C and D). Compared with F127/Cur, MAP-F127/Cur induced less alteration in skin structure, which may be attributed to the bioadhesive property of MAP. Following application of MAP-F127/Cur to the skin, the bioadhesive properties of MAP enable the drug carrier to adhere tightly to the skin and create a protective film, thereby enhancing the barrier functions of the skin.[57] In addition, upon contact of the MAP-F127/Cur with skin, the MAP coating might promote the repair of epidermal barrier by conducting nonspecific cell adhesion and establishing a network scaffold through electrostatic interactions or van der Waals forces.[58] Histological examination showed no cell necrosis or inflammatory cell infiltration, suggesting that MAP-F127/Cur may have good biological safety.

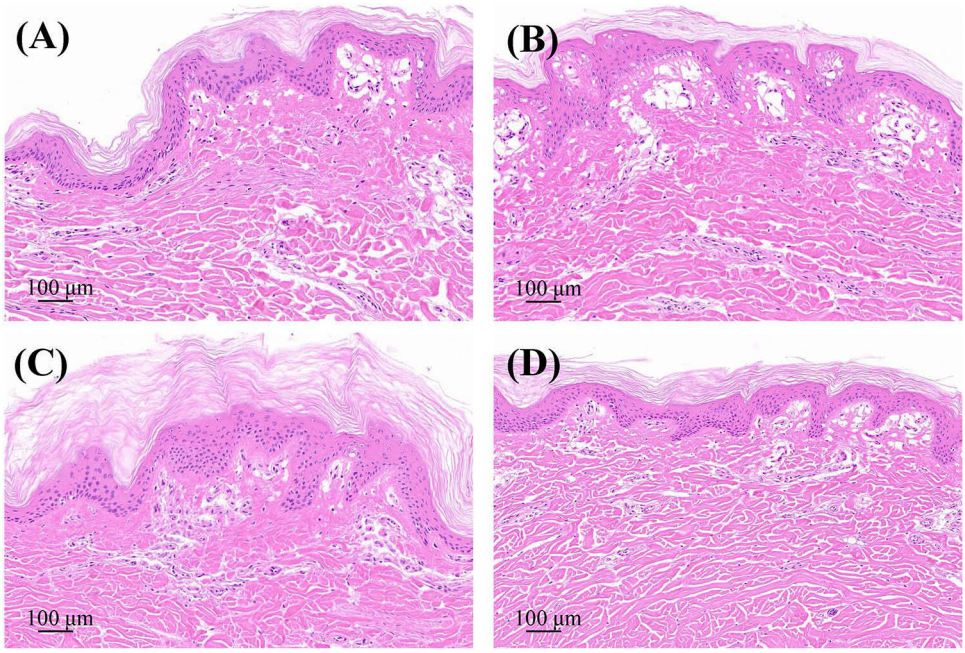

Figure 9 HE staining of the skin treated with (**A**) physiological saline, (**B**) Cur solution, (**C**) F127/Cur and (**D**) MAP-F127/Cur.

Interaction Mechanism of the Micelles with Skin

Figure 10A shows the SEM images of the skin samples treated with different formulations. The skin surface exposed to physiological saline exhibited smooth and intact morphological characteristics, whereas treatment with Cur solution resulted in slight loosening of the SC. Both F127/Cur and MAP-F127/Cur caused significant number of fragments crumpled and detached from the skin surface, demonstrating their capacity to disrupt the highly organized and dense arrangement of the SC and consequently enhance skin permeability. Notably, MAP-F127/Cur treatment resulted in reduced damage to the SC compared to F127/Cur treatment, which could be ascribed to the capacity of MAP to restore the damaged skin barrier function.[59] DSC analysis corroborated the SEM findings, revealing keratin melting peaks at 76.2 °C for physiological saline treated skin, which shifted to higher temperatures of 93.03 °C and 91.07 °C following F127/Cur and MAP-F127/Cur treatments, respectively (Figure 10B), indicating that micellar formulations can alter the molecular structure of keratin. FTIR analysis revealed characteristic peaks for control skin, with amide I and II bands of keratin at 1631 cm^{-1} and 1542 cm^{-1}, respectively, along with symmetric and asymmetric stretching vibration peaks of the lipid alkyl chain at 2852 cm^{-1} and 2921 cm^{-1}, respectively (Figure 10C). Treatment with F127/Cur and MAP-F127/Cur significantly attenuated these characteristic peaks, demonstrating their ability to modify keratin conformation and disrupt the ordered structure of the SC, consequently enhancing skin permeability.[60]

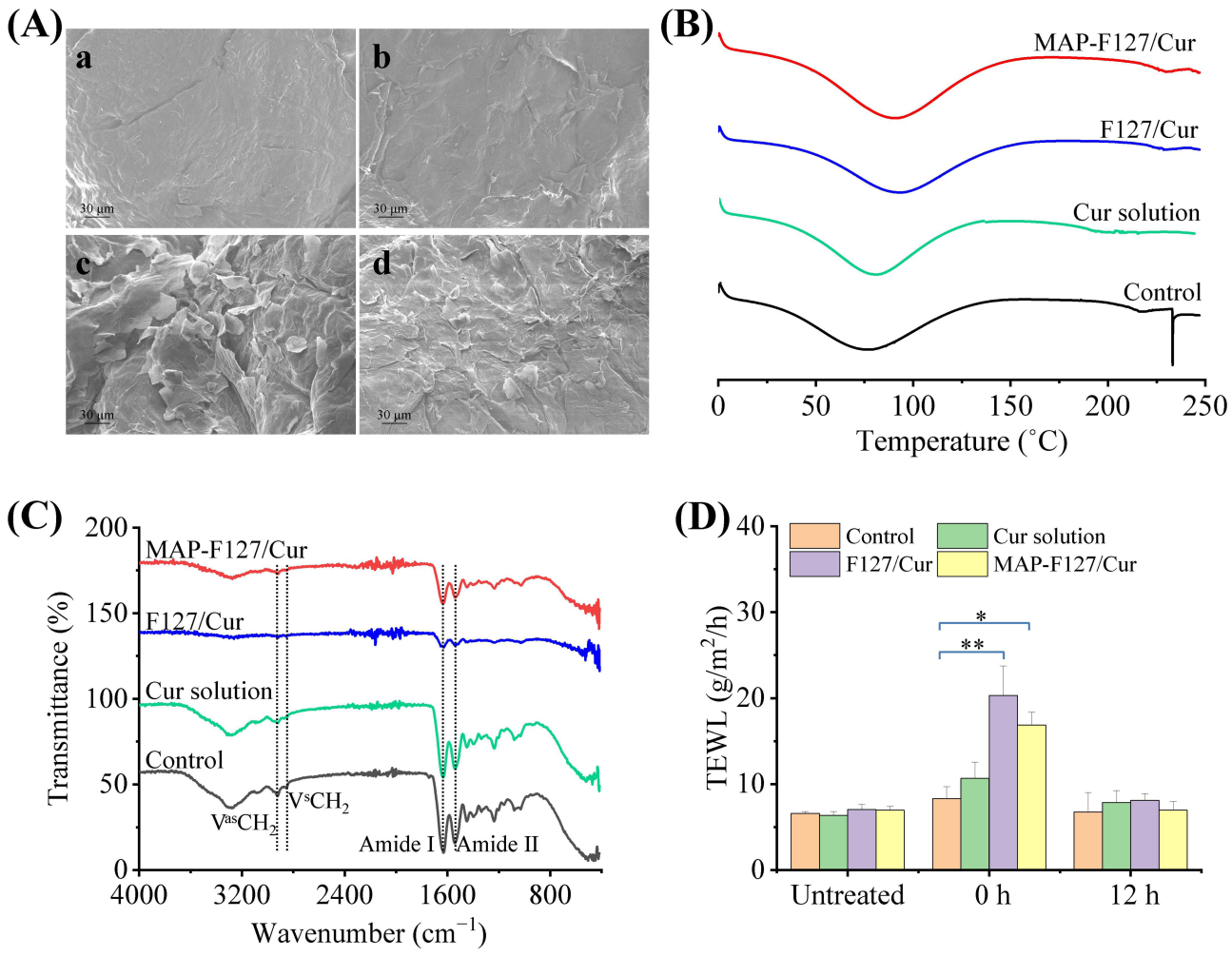

Figure 10 (**A**) SEM photomicrographs of porcine skin samples treated with (a) physiological saline, (b) Cur solution, (c) F127/Cur and (d) MAP-F127/Cur (Scale bar: 30 μm). (**B**) The DSC curves and (**C**) FTIR spectra of porcine skin samples treated with various formulations. (**D**) Effect of various formulations on TEWL values (n=3; *$p < 0.05$, **$p < 0.01$).

https://doi.org/10.2147/IJN.S563465

TEWL is a key parameter for evaluating skin barrier function, and changes in its values directly reflect the degree of skin barrier damage. The effects of different formulations on skin barrier integrity were evaluated by measuring changes in TEWL values before and after administration. The results showed that both F127/Cur and MAP-F127/Cur treatments caused a significant increase in TEWL values after 12 h (Figure 10D), which might be due to the extraction and dissolution of skin lipids by micelles, resulting in disruption of the barrier structure.[61] Although both formulations elevated TEWL, the increase was less pronounced with MAP-F127/Cur than with F127/Cur. This difference could be attributed to the protective film formed by the adhesive MAP on the skin surface, which can effectively reduce water evaporation[58] It was noted that the TEWL values of all treatment groups returned to normal levels after 24 h, indicating that the damaging effect of the micellar formulation on the skin barrier is reversible. In conclusion, MAP-F127/Cur can temporarily disrupt the structure of lipids in the skin barrier and the molecular conformation of keratin, thereby enhancing the efficiency of transdermal drug absorption.

Therapeutic Effect of Psoriasis in Mice

Figure 11A shows the establishment of the mouse psoriasis model and the administration strategy. From the perspective of the development of skin inflammation, except for the normal group, the psoriasis-related scores (erythema, scales, skin thickening and comprehensive score) of the other groups all rose to the highest level on the 6th day of modeling, and then began to decline (Figure 11B). To the experimental termination date (day 8), all treatment groups demonstrated significantly reduced scores for each index compared to the model group ($p < 0.001$). Both F127/Cur and MAP-F127 /Cur could effectively relieve the symptoms of skin lesions, and the score of MAP-F127/Cur group decreased more significantly, indicating that MAP modification significantly enhanced anti-inflammatory efficacy of Cur in the IMQ-induced psoriasis-like mouse model by improving its skin absorption.

The observation of skin apparent symptoms showed that the skin of mice exhibited obvious skin shrinkage, dryness and slight thickening in all experimental groups except normal controls from the second day. The severity of dermatological manifestations in the model group increased progressively with prolonged modeling duration. The skin lesions of the mice in the model group continued to deteriorate with the modeling time. A large number of scales appeared on the back, and the skin presented a hardened and thickened state. Compared to untreated model animals, therapeutic intervention with Cur formulations significantly ameliorated back skin scaling, thickening, and erythematous changes. The mice in the Cur solution treatment group still had obvious scales on the back on day 8, while the inflammation of the mice was relieved after treatment with MAP-F127/Cur and F127/Cur, and the relief effect of skin inflammation was more obvious in the MAP-F127/Cur group (Figure 11C). The HE staining results revealed well-organized epidermal and dermal structures in the normal control group. The model group presented typical lesion characteristics of psoriasis, including excessive keratinization, incomplete keratinization, epidermal hyperplasia and elongated epidermal nail processes. Epidermal thickening was significantly reduced in both the MAP-F127/Cur and F127/Cur treatment groups, but elongated epidermal nail processes was still observed. Among all Cur preparations, the anti-inflammatory effect of the MAP-F127/Cur group was the most prominent, and the histological state of the skin tended to be normalized. We subsequently quantified the thickness of epidermis of mice across all experimental groups. The model group displayed an epidermal thickness of 78 μm, while administration of Cur solution and F127/Cur led to a reduction in thickness of epidermis, with values falling to 65 μm and 40 μm, respectively. More strikingly, the MAP-F127/Cur treatment group exhibited a further decrease to 18 μm, only about 3 μm greater than the 15 μm in the normal group (Figure 11D). These results demonstrate that MAP-F127/Cur treatment not only effectively normalized the thickness of epidermis but also supported the reestablishment of a typical undulating epidermal border and ameliorated pathological thickening of the spinous layer. It is noteworthy that although MAP-F127/Cur demonstrated significant efficacy in improving psoriasiform skin lesions, reducing PASI scores, and suppressing keratinocyte hyperproliferation, its therapeutic effect was still inferior to that of the positive control drug CP. This difference primarily stems from the potent action of CP as a super-high-potency glucocorticoid. However, long-term use of such high-potency steroids carries the risk of adverse effects like skin atrophy. Therefore, the MAP-F127/Cur holds promise as a safer therapeutic alternative.

The splenic tissue comparison and spleen index of each group were respectively shown in Figure 11E and F. Pathological assessment revealed substantial spleen size expansion in model animals, with calculated spleen index

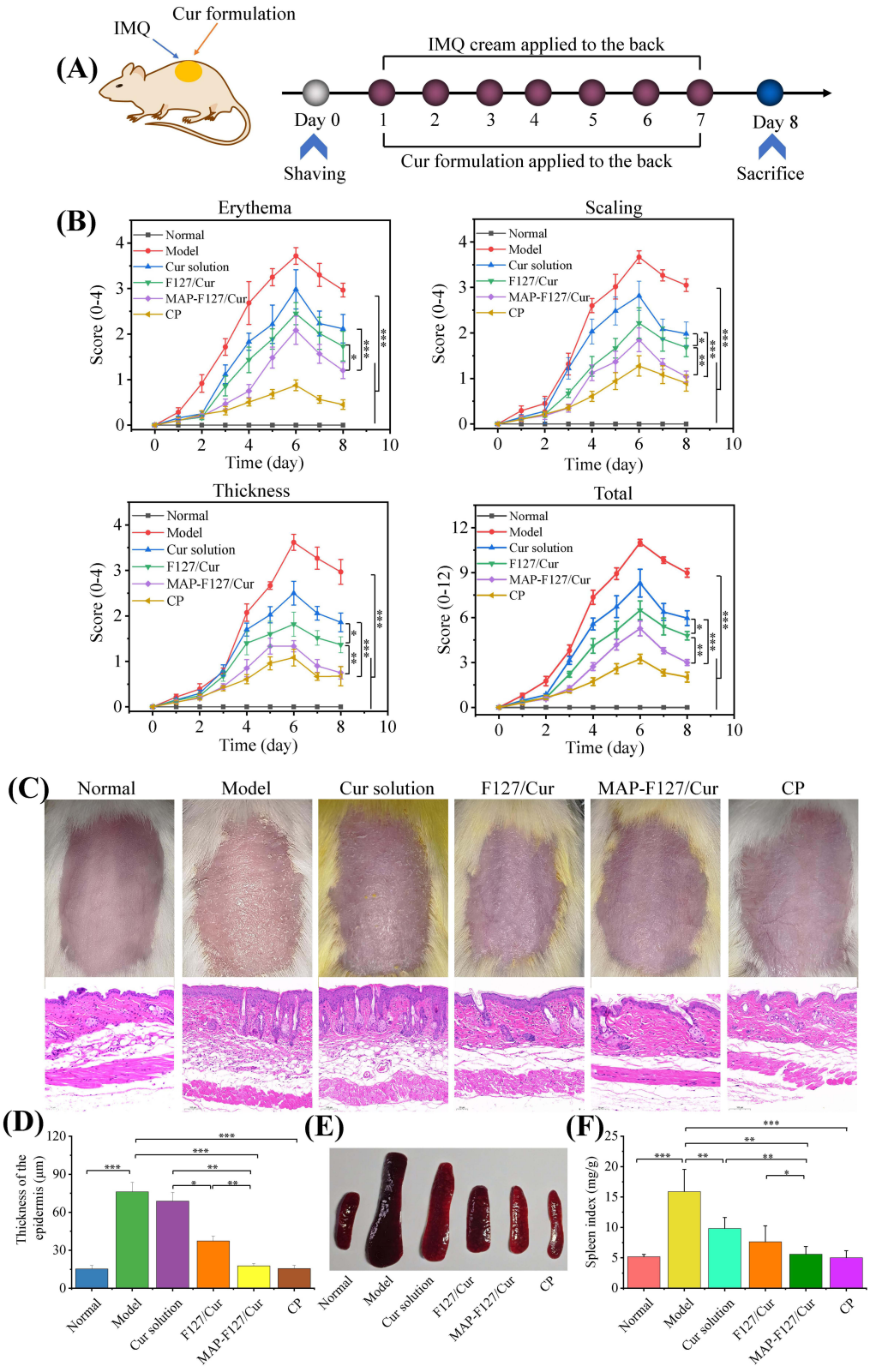

Figure 11 Effect of topical administration in the treatment of psoriasis. (**A**) Administration timeline. (**B**) PASI score on the back of mice. (**C**) Observation of skin lesions on the back of mice and histological evaluation of the back skin. (**D**) Thickness of epidermis of mice determined via HE staining analysis. (**E**) Representative image of the spleen of mice. (**F**) Spleen index of mice (n=6; *$p < 0.05$, **$p < 0.01$, ***$p < 0.001$).

https://doi.org/10.2147/IJN.S563465

significantly exceeding those of normal group mice. Research had demonstrated that IMQ could promote spleen enlargement by expanding immune cell populations and inducing comprehensive changes in splenocyte composition.[62] The spleen index observed after topical administration of MAP-F127/Cur were significantly reduced compared with that of unmodified F127/Cur ($p < 0.05$), suggests that the MAP-modified formulation may attenuate systemic inflammation in the IMQ-induced psoriasis-like mouse model. This effect may be attributed to the ability of MAP-F127/Cur to down-regulate the expression of pro-inflammatory factors at the local lesion site, thereby blocking the transmission of local inflammatory signals to the systemic circulation and indirectly mitigating the compensatory splenomegaly caused by systemic inflammation.[63] Given that mouse models of psoriasis cannot perfectly replicate the chronic, spontaneous nature and complexity of the human disease, our future research will involve the development of superior disease models combined with a multi-dimensional pharmacodynamic evaluation system for in-depth investigation.

Conclusions

This study developed a mussel adhesive protein (MAP)-modified Pluronic F127 micelle (MAP-F127/Cur) to enhance the topical cutaneous delivery of Cur. Through in vitro experiments, we confirmed that this bioadhesion-inspired micellar system can effectively permeate the skin via the SC, hair follicles, and other skin appendage pathways, while achieving substantial retention in skin tissue. In vivo studies further demonstrated that MAP-F127/Cur significantly alleviated both the symptoms and histopathological manifestations in imiquimod (IMQ)-induced psoriasis-like mice. These findings provide valuable insights for research on the topical administration of Cur in the treatment of inflammation-related skin diseases.

Ethics Declaration

All animal experiments were approved by the Animal Ethics Committee of Luoyang Normal University (protocol code: LYNUIACUA–2025–03.217–069) and were performed in accordance with the guidelines of Regulations on the Administration of Laboratory Animals in Henan Province. At the end of the experimental period, animals were humanely euthanized by intraperitoneal injection of an overdose of sodium pentobarbital (150 mg/kg). Death was confirmed by the absence of corneal reflex and cessation of heartbeat.

Funding

This study was supported by the National Natural Science Foundation of China (32101150), the Key Scientific Research Project of Higher Education of Henan Province (23A350002), the Key Scientific and Technological Project of Henan Province of China (242102110051), and the Innovative training program for college students (202510482041 and 202510482055).

Disclosure

The authors declare no conflict of interest.

References

1. Saw PE, Song E. The 'inflammazone' in chronic inflammatory diseases: psoriasis and sarcoidosis. *Trends Immunol*. 2025;46(2):121–137. doi:10.1016/j.it.2025.01.002
2. Huang C, Li W, Shen C, et al. YAP1 facilitates the pathogenesis of psoriasis via modulating keratinocyte proliferation and inflammation. *Cell Death Dis*. 2025;16(1):186. doi:10.1038/s41419-025-07521-3
3. Pan W, Shi Y, Sun F, et al. Oleogel-mediated topical administration of roflumilast and paclitaxel as a synergistic strategy to combat imiquimod-induced psoriasis. *AAPS Pharm Sci Tech*. 2025;26(5):127. doi:10.1208/s12249-025-03118-3
4. Sood A, Tikoo K. Topical delivery of pterostilbene nanoemulgel ameliorates imiquimod-induced psoriasis-like skin inflammation in mice. *Nanomedicine*. 2025;20(8):791–802. doi:10.1080/17435889.2025.2480047
5. Yang N, Ai X, Cheng K, et al. A compound essential oil alters stratum corneum structure, potentially promoting the transdermal permeation of hydrophobic and hydrophilic ingredients. *Curr Drug Deliv*. 2024;21(5):744–752. doi:10.2174/1567201820666230120122206
6. Lu B, Zhong Y, Zhang J, et al. Curcumin-based ionic liquid hydrogel for topical transdermal delivery of curcumin to improve its therapeutic effect on the psoriasis mouse model. *ACS Appl Mater Interfaces*. 2024;16(14):17080–17091. doi:10.1021/acsami.3c17091
7. Lu B, Zhang J, Zhang J. Enhancing transdermal delivery of curcumin-based ionic liquid liposomes for application in psoriasis. *ACS Appl Bio Mater*. 2023;6(12):5864–5873. doi:10.1021/acsabm.3c01026

8. Ahmad A, Akhtar J, Ahmad M, et al. Curcumin nanogel preparations: a promising alternative for psoriasis treatment. *Curr Drug Metab*. 2024;25(3):179–187. doi:10.2174/0113892002312605240508042634
9. Yao L, Tian F, Meng Q, et al. Reactive oxygen species-responsive supramolecular deucravacitinib self-assembly polymer micelles alleviate psoriatic skin inflammation by reducing mitochondrial oxidative stress. *Front Immunol*. 2024;15:1407782. doi:10.3389/fimmu.2024.1407782
10. Lei Y, Jiang W, Peng C, et al. Advances in polymeric nano-delivery systems targeting hair follicles for the treatment of acne. *Drug Deliv*. 2024;31(1):2372269. doi:10.1080/10717544.2024.2372269
11. An P, Zhao Q, Hao S, et al. Recent advancements and trends of topical drug delivery systems in psoriasis: a review and bibliometric analysis. *Int J Nanomed*. 2024;19:7631–7671. doi:10.2147/IJN.S461514
12. Niu J, Yuan M, Chen C, et al. Berberine-loaded thiolated pluronic F127 polymeric micelles for improving skin permeation and retention. *Int J Nanomed*. 2020;15:9987–10005. doi:10.2147/IJN.S270336
13. Ni P, Chen Y, Wan K, et al. Mussel foot protein-inspired adhesive tapes with tunable underwater adhesion. *ACS Appl Mater Interfaces*. 2024;16(34):45550–45562. doi:10.1021/acsami.4c09709
14. Xue R, Zhang M, Zhang C, et al. Molecular simulations guiding recombinant mussel protein with enhanced applicable properties for adhesive materials. *Int J Biol Macromol*. 2025;307(Pt 2):141988. doi:10.1016/j.ijbiomac.2025.141988
15. Yang JW, Yoon T, Kim H, et al. Acrylated bioengineered mussel protein-based adhesive nanoparticles for locoregional and sustained drug delivery. *ACS Biomater Sci Eng*. 2025;11(6):3523–3532. doi:10.1021/acsbiomaterials.5c00390
16. Jeong Y, Jo YK, Kim BJ, et al. Sprayable adhesive nanotherapeutics: mussel-protein-based nanoparticles for highly efficient locoregional cancer therapy. *ACS Nano*. 2018;12(9):8909–8919. doi:10.1021/acsnano.8b04533
17. Ye LP, Huang WQ, Deng YH, et al. Development of a pluronic-zein-curcumin drug delivery system with effective improvement of hydrophilicity, stability and sustained-release. *J Cereal Sci*. 2022;104:103412. doi:10.1016/j.jcs.2022.103412
18. Mao Y, Hao T, Zhang H, et al. Penetration enhancer-free mixed micelles for improving eprinomectin transdermal c efficiency in animal parasitic infections therapy. *Int J Nanomed*. 2024;19:11071–11085. doi:10.2147/IJN.S476164
19. Alhur SJA, Mahmood HS. Fabrication and assessment of ethosomes for effective transdermal delivery of loxoprofen. *Iran J Basic Med Sci*. 2025;28(6):728–738. doi:10.22038/ijbms.2025.84183.18206
20. Niu J, Yuan M, Gao P, et al. Microemulsion-based keratin-chitosan gel for improvement of skin permeation/retention and activity of curcumin. *Gels*. 2023;9(7):587. doi:10.3390/gels9070587
21. Baldassa MAB, Dias RVR, Oliveira LC, et al. Aqueous mixtures of cornstarch and Pluronic(R) F127 studied by experimental and computational techniques. *Food Res Int*. 2022;158:111515. doi:10.1016/j.foodres.2022.111515
22. Wu TY, Huang CC, Tsai HC, et al. Mucin-mediated mucosal retention via end-terminal modified Pluronic F127-based hydrogel to increase drug accumulation in the lungs. *Biomater Adv*. 2024;156:213722. doi:10.1016/j.bioadv.2023.213722
23. Chen S, Shen B, Zhang F, et al. Mussel-inspired graphene film with enhanced durability as a macroscale solid lubricant. *ACS Appl Mater Interfaces*. 2019;11(34):31386–31392. doi:10.1021/acsami.9b10404
24. Hu C, Wang J, Gao X, et al. Pluronic-based nanoparticles for delivery of doxorubicin to the tumor microenvironment by binding to macrophages. *ACS Nano*. 2024;18(22):14441–14456. doi:10.1021/acsnano.4c01120
25. Sk Mosiur R, Dutta G, Biswas R, et al. Succinyl curcumin conjugated chitosan polymer-prodrug nanomicelles: a potential treatment for Type-II diabetes in diabetic Balb/C mice. *Acta Chim Slov*. 2024;71(2):421–435. doi:10.17344/acsi.2024.8658
26. Zhao X, Luo J, Huang Y, et al. Injectable antiswelling and high-strength bioactive hydrogels with a wet adhesion and rapid gelling process to promote sutureless wound closure and scar-free repair of infectious wounds. *ACS Nano*. 2023;17(21):22015–22034. doi:10.1021/acsnano.3c08625
27. Pham DT, Phewchan P, Navesit K, et al. Development of metronidazole-loaded *in situ* thermosensitive hydrogel for periodontitis treatment. *Turk J Pharm Sci*. 2021;18(4):510–516. doi:10.4274/tjps.galenos.2020.09623
28. Cao X, He Q, Adu-Frimpong M, et al. Preparation of pinocembrin-loaded F127/MPEG-PDLLA polymer micelles and anti-osteoporotic activity. *AAPS Pharm Sci Tech*. 2022;23(7):276. doi:10.1208/s12249-022-02427-1
29. Liu Y, Huang P, Hou X, et al. Hybrid curcumin-phospholipid complex-near-infrared dye oral drug delivery system to inhibit lung metastasis of breast cancer. *Int J Nanomed*. 2019;14:3311–3330. doi:10.2147/IJN.S200847
30. Lv J, Zhou X, Wang W, et al. Solubilization mechanism of self-assembled walnut protein nanoparticles and curcumin encapsulation. *J Sci Food Agric*. 2023;103(10):4908–4918. doi:10.1002/jsfa.12559
31. Ali MK, Moshikur RM, Wakabayashi R, et al. Biocompatible ionic liquid-mediated micelles for enhanced transdermal delivery of paclitaxel. *ACS Appl Mater Interfaces*. 2021;13(17):19745–19755. doi:10.1021/acsami.1c03111
32. Li Q, Lianghao Y, Shijie G, et al. Self-assembled nanodrug delivery systems for anti-cancer drugs from traditional Chinese medicine. *Biomater Sci*. 2024;12(7):1662–1692. doi:10.1039/D3BM01451G
33. Tian YY, Zhang XH, Huang YQ, et al. Amphiphilic prodrug nano-micelles of fipronil coupled with natural carboxylic acids for improving physicochemical properties and reducing the toxicities to aquatic organisms. *Chem Eng J*. 2022;439:135717. doi:10.1016/j.cej.2022.135717
34. Wu S, Geng F, He S, et al. Amphiphilic poly(caprolactone-b-N-hydroxyethyl acrylamide) micelles for controlled drug delivery. *RSC Adv*. 2020;10(50):29668–29674. doi:10.1039/D0RA01473G
35. Wang F, Li Y, Yu L, et al. Amphiphilic mPEG-Modified oligo-phenylalanine nanoparticles chemoenzymatically synthesized via papain. *ACS Omega*. 2020;5(46):30336–30347. doi:10.1021/acsomega.0c05076
36. Niu J, Yuan M, Liu Y, et al. Silk peptide-hyaluronic acid based nanogels for the enhancement of the topical administration of curcumin. *Front Chem*. 2022;10:1028372. doi:10.3389/fchem.2022.1028372
37. Niu J, Yuan M, Li H, et al. Pentapeptide modified ethosomes for enhanced skin retention and topical efficacy activity of indomethacin. *Drug Deliv*. 2022;29(1):1800–1810. doi:10.1080/10717544.2022.2081739
38. Dawud H, Abu Ammar A. Rapidly dissolving microneedles for the delivery of steroid-loaded nanoparticles intended for the treatment of inflammatory skin diseases. *Pharmaceutics*. 2023;15(2):526. doi:10.3390/pharmaceutics15020526
39. Al Fatease A, Alqahtani A, Khan BA, et al. Preparation and characterization of a curcumin nanoemulsion gel for the effective treatment of mycoses. *Sci Rep*. 2023;13(1):22730. doi:10.1038/s41598-023-49328-2
40. Abu-Much A, Darawshi R, Dawud H, et al. Preparation and characterization of flexible furosemide-loaded biodegradable microneedles for intradermal drug delivery. *Biomater Sci*. 2022;10(22):6486–6499. doi:10.1039/D2BM01143C

41. Yuan M, Niu J, Li F, et al. Dipeptide-1 modified nanostructured lipid carrier-based hydrogel with enhanced skin retention and topical efficacy of curcumin. *RSC Adv*. 2023;13(42):29152–29162. doi:10.1039/D3RA04739C
42. Liu CH, Lee GW, Wu WC, et al. Encapsulating curcumin in ethylene diamine-β-cyclodextrin nanoparticle improves topical cornea delivery. *Colloids Surf B Biointerfaces*. 2020;186:110726. doi:10.1016/j.colsurfb.2019.110726
43. Gutierrez-Saucedo RA, Gomez-Lopez JC, Villanueva-Briseno AA, et al. Pluronic F127 and P104 polymeric micelles as efficient nanocarriers for loading and release of single and dual antineoplastic drugs. *Polymers (Basel)*. 2023;15(10):2249. doi:10.3390/polym15102249
44. Omidian H, Wilson RL. Long-acting gel formulations: advancing drug delivery across diverse therapeutic areas. *Pharmaceuticals*. 2024;17(4):19. doi:10.3390/ph17040493
45. Sunoqrot S, Orainee B, Alqudah DA, et al. Curcumin-tannic acid-poloxamer nanoassemblies enhance curcumin's uptake and bioactivity against cancer cells in vitro. *Int J Pharm*. 2021;610:121255. doi:10.1016/j.ijpharm.2021.121255
46. Meng R, Wu Z, Xie QT, et al. Preparation and characterization of zein/carboxymethyl dextrin nanoparticles to encapsulate curcumin: physico-chemical stability, antioxidant activity and controlled release properties. *Food Chem*. 2021;340:127893. doi:10.1016/j.foodchem.2020.127893
47. Zhang Y, Xia Q, Li Y, et al. CD44 assists the topical anti-psoriatic efficacy of curcumin-loaded hyaluronan-modified ethosomes: a new strategy for clustering drug in inflammatory skin. *Theranostics*. 2019;9(1):48–64. doi:10.7150/thno.29715
48. Darade AR, Lapteva M, Ling V, et al. Polymeric micelles for cutaneous delivery of the hedgehog pathway inhibitor TAK-441: formulation development and cutaneous biodistribution in porcine and human skin. *Int J Pharm*. 2023;644:123349. doi:10.1016/j.ijpharm.2023.123349
49. Cui G, Guo X, Deng L. Preparation strategies of mussel-inspired chitosan-based biomaterials for hemostasis. *Front Pharmacol*. 2024;15:1439036. doi:10.3389/fphar.2024.1439036
50. Dai Q, Liu H, Gao C, et al. Advances in mussel adhesion proteins and mussel-inspired material electrospun nanofibers for their application in wound repair. *ACS Biomater Sci Eng*. 2024;10(10):6097–6119. doi:10.1021/acsbiomaterials.4c01378
51. Yu C, Wang M, Zhang D, et al. Mussel-inspired robust and waterproof soybean protein adhesives enhanced with phenolated lignosulfonate for wood bonding. *Int J Biol Macromol*. 2025;314:144419. doi:10.1016/j.ijbiomac.2025.144419
52. Jiamphun S, Chaiyana W. Enhancing skin delivery and stability of vanillic and ferulic acids in aqueous enzymatically extracted glutinous rice husk by nanostructured lipid carriers. *Pharmaceutics*. 2023;15(7):1961. doi:10.3390/pharmaceutics15071961
53. Chen Y, Wu Q, Zhang Z, et al. Preparation of curcumin-loaded liposomes and evaluation of their skin permeation and pharmacodynamics. *Molecules*. 2012;17(5):5972–5987. doi:10.3390/molecules17055972
54. Di Filippo LD, de Paula MC, Duarte JL, et al. Nanocarrier functionalization strategies for targeted drug delivery in skin cancer therapy: current progress and upcoming challenges. *Expert Opin Drug Delivery*. 2023;20(6):831–849. doi:10.1080/17425247.2023.2221026
55. Shi TT, Lv YJ, Huang WZ, et al. Enhanced transdermal delivery of curcumin nanosuspensions: a mechanistic study based on co-localization of particle and drug signals. *Int J Pharm*. 2020;588:119737. doi:10.1016/j.ijpharm.2020.119737
56. Bachhav YG, Mondon K, Kalia YN, et al. Novel micelle formulations to increase cutaneous bioavailability of azole antifungals. *J Control Release*. 2011;153(2):126–132. doi:10.1016/j.jconrel.2011.03.003
57. Wang YM, Xiao DD, Quan L, et al. Mussel-inspired adhesive gelatin-polyacrylamide hydrogel wound dressing loaded with tetracycline hydrochloride to enhance complete skin regeneration. *Soft Matter*. 2022;18(3):662–674. doi:10.1039/D1SM01373D
58. Dong RC, Jin QM, Zhi JH, et al. Mussel adhesive protein treatment delivered by microneedling for sensitive skin: a clinical study. *J Cosmet Dermatol*. 2023;22(6):1835–1843. doi:10.1111/jocd.15645
59. Luo Y, Nan M, Dong R, et al. Rosacea treatment with mussel adhesive protein delivered via microneedling: in vivo and clinical studies. *J Cosmet Dermatol*. 2024;23(5):1654–1662. doi:10.1111/jocd.16190
60. Yi QF, Yan J, Tang SY, et al. Effect of borneol on the transdermal permeation of drugs with differing lipophilicity and molecular organization of stratum corneum lipids. *Drug Dev Ind Pharm*. 2016;42(7):1086–1093. doi:10.3109/03639045.2015.1107095
61. Makhmalzade BS, Chavoshy F. Polymeric micelles as cutaneous drug delivery system in normal skin and dermatological disorders. *J Adv Pharm Technol Res*. 2018;9(1):2–8. doi:10.4103/japtr.JAPTR_314_17
62. Wang Y, Han D, Huang Y, et al. Oral administration of punicalagin attenuates imiquimod-induced psoriasis by reducing ROS generation and inflammation via MAPK/ERK and NF-kappaB signaling pathways. *Phytother Res*. 2024;38(2):713–726. doi:10.1002/ptr.8071
63. Ahmad MZ, Mohammed AA, Algahtani MS, et al. Nanoscale topical pharmacotherapy in management of psoriasis: contemporary research and scope. *J Funct Biomater*. 2022;14(1):19. doi:10.3390/jfb14010019